Journal Name

ARTICLE

Large Area Quantum Dot Luminescent Solar Concentrators for Use with Dye-Sensitised Solar Cells

Received 00th January 20xx,
Accepted 00th January 20xx

DOI: 10.1039/x0xx00000x

www.rsc.org/

Lorcan J. Brennan[a], Finn Purcell-Milton[a⊥], Barry McKenna[a⊥] Trystan M. Watson[c], Yurii K. Gun'ko[a,b], and Rachel C. Evans*[a,d]

Luminescent solar concentrators (LSCs) have the potential to significantly contribute to solar energy harvesting strategies in the built environment. For the practical realisation of LSC technology, the ability to create large area devices, which contain considerable volumes of high quality luminescent species, is paramount. Here, we report the development of large area (90 cm^2 top face), planar LSCs doped with green-emitting CdSe@ZnS/ZnS core-shell quantum dots (QD) with a composition gradient shell. The champion LSC demonstrates an optical efficiency of 1.2 %, for a geometric factor of 7.9, under full spectrum illumination (AM1.5 G). It was observed that inhomogeneity in the edge emission is a feature of large area devices and that an appropriate measurement geometry should be used to account for this when determining the optical efficiency. The LSCs exhibit excellent optical stability under accelerated testing conditions and display reasonably low optical reabsorption losses. Proof-of-principle integration of the QD-LSC with a planar, thin strip DSSC is demonstrated to generate a enhanced photocurrent. These results not only highlight the promise of composition gradient shell QDs for the practical realisation of large area LSCs, but indicate that we should look beyond conventional silicon cells and towards emerging photovoltaic (PV) technologies for the design of hybrid LSC-PV systems for the urban environment.

Introduction

With the ever-increasing demand for society to move away from fossil fuel sources, our approach to sustainable energy generation must become tailored to the requirements of the modern, urban population. The next generation of energy-harvesting devices cannot be solely confined to conventional solar or wind farms, but should be seamlessly integrated into modern architecture, in the development of zero- or low-energy consumption buildings of the future. Luminescent solar concentrators (LSCs) are poised to play an important role in this transition, with the potential to serve as transparent or semi-transparent solar harvesting windows and daylighting systems for building integrated photovoltaic (BIPV) technology.[1-8] An LSC typically consists of a transparent polymeric waveguide slab, which is doped with a highly luminescent species, capable of absorbing large portions of the solar spectrum. The luminophore absorbs incident sunlight, reemitting it at longer wavelengths. Reemitted photons are captured by the waveguide and transported to the edge of the waveguide *via* total internal reflection (**Figure 1**). The light arriving at the edge of the waveguide is thus highly concentrated, given that the large area, top surface of the waveguiding plate captures and concentrates light to the much smaller edge area. This concentrated light can then be used to generate electricity, through integration of the LSC with an appropriate PV cell.

Although the concept of the LSC was first proposed in the 1970s,[9, 10] recent advances in novel classes of fluorescent and phosphorescent materials with superior optical properties (high photoluminescence quantum yields, large Stokes' shifts, broad absorption windows) have reinvigorated this area of research.[1, 2, 11, 12] Conventional conjugated organic molecular

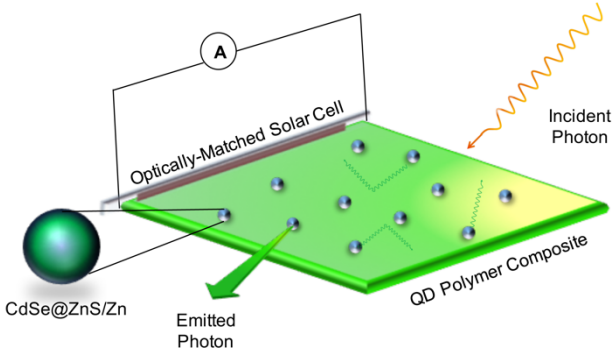

Figure 1. Schematic operation of a QD-doped LSC coupled to a solar cell. Incident photons (orange) falling on the top face of the LSC excite green-emitting CdSe@ZnS/ZnS QDs embedded within the polymer waveguide. Emitted light (green arrow) is guided towards the edges of the slab *via* total internal reflection. The concentrated light is used to illuminate an optically-matched integrated solar cell, resulting in the generation of photocurrent.

[a] School of Chemistry and CRANN, Trinity College, The University of Dublin, Dublin 2, Ireland
[b] ITMO University, 197101 St. Petersburg, Russia
[c] SPECIFIC – College of Engineering, Swansea University, Bay Campus, Swansea, SA1 8EN, U.K.
[d] Department of Materials Science & Metallurgy, University of Cambridge, U.K.
E-mail: rce26@cam.ac.uk
⊥ These authors contributed equally to this work.
Electronic Supplementary Information (ESI) available: Further details of LSC and DSSC fabrication; further characterisation of QDs (TEM, EDX, TGA, emission quantum yield), experimental set-up for LSC characterisation, calculation of theoretical maximum LSC efficiency, optical power data for edge emission. See DOI: 10.1039/x0xx00000x

luminophores used in LSCs, such as perylene carboxdiimides,[5, 13-18] have increasingly been replaced with more exotic species, such as colloidal quantum dots (QDs) and nanocrystals,[1, 2, 6, 12, 19] metal complexes[20-22] and aggregation-induced emitters.[23, 24] Quantum dots, in particular, are attractive for LSCs due to the possibility of engineering their photophysical properties through judicious choice of the material/architecture combination employed (*e.g.* by forming core/shell[25], alloyed[26] or doped QD structures).[27, 28] This structural versatility allows not only access to high resistance to photobleaching and judicious control of the Stokes shift and emission quantum yield, but also results in a tuneable band-gap energy, which can be tailored to absorb and emit light across the entire UV/visible/NIR region. This affords the unique opportunity to couple QD-LSCs to different types of solar cells, and also allows for a variety of device colours, making them an attractive option for aesthetically-pleasing architectural designs. Moreover, the QD surface can be readily modified, enabling easy integration of QDs into a range of polymeric matrices.[29, 30]

Recent efforts on QD and nanocrystal LSCs have focussed on the use of band-gap and Stokes-shift engineering to minimise optical losses resulting from the reabsorption of emitted photons by neighbouring fluorophores. Lunt *et al*. reported that hexanuclear metal halide nanoclusters of the form $M_6(II)X_{12}$ (M = Mo, W, X = Cl, Br, I) encapsulated in poly(butyl methacrylate-*co*-methacrylate)/poly(ethylmethacrylate) composites exhibited a massive Stokes shift of ~400 nm and could sensitise a coupled Si cell module.[31] More recently, LSCs incorporating band-gap engineered Mn^{2+}-doped ZnSe/ZnS core-shell quantum dots which exhibited zero reabsorption for device dimensions of 25 × 75 × 0.42 mm have been reported.[32]

Optical losses become prevalent as devices are scaled to the sizes needed for practical implementation in the built environment, where photon transport is necessary over macroscopic distances.[19] However, to date, there have in fact been relatively few studies on the fabrication and characterisation of three-dimensional (3D) large-area QD-LSCs that more realistically reflect the challenges associated with scaling-up this technology. Meinardi *et al*. applied 'Stokes-shift-engineered' core-shell CdSe/CdS nanocrystals in the development of large-area (10 cm × 1.5 cm × 0.2 cm) QD-LSCs, which exhibited an optical efficiency of ~10.2 % under A.M 1.5G illumination (100 mW cm^{-2}), employing white diffusing reflectors along the long faces of the waveguide to amplify the output.[2] The same group subsequently developed colourless LSCs (12 cm × 12 cm × 0.3 cm) employing heavy-metal free $CuInSe_xS_{2-x}$ QDs embedded in a poly(laurylmethacrylate) and ethylene glycol dimethacrylate co-polymer (pLMA-*co*-EGDM), with a reported optical power efficiency of 3.2 % in the absence of light diffusers or reflectors.[1] More recently, Rosei *et al.* have also demonstrated that rectangular near-IR LSCs (5 cm × 1.5 cm × 0.3 cm) can be fabricated utilising PbS/CdS core/shell QDs in pLMA-*co*-EGDM, with a reported optical efficiency of 6.1%.[33]

Although Stokes-shift engineering has enabled reabsorption losses to be overcome to to some extent, significant challenges still remain for the practical realisation of QD-LSC devices. These include the development of synthetic methodologies to enable the incorporation of high QD dopant concentrations, the design of 3D large-area prototypes of sufficient optical quality and the introduction of standardised characterisation methods to ensure reproducible reporting of the optical efficiency. Moreover, LSCs and spectral conversion approaches in general have been relatively overlooked for implementation with third generation photovoltaic devices such as dye-sensitised solar cells (DSSCs)[34-36] and perovskite solar cells.[37] To address these limitations, here we report the fabrication of large-area LSCs by dispersion of green-emitting CdSe@ZnS/ZnS QDs with a composition gradient shell[38] in a pLMA-*co*-EGDM matrix. CdSe@ZnS/ZnS QDs were selected as the luminophore due to their high photoluminescence quantum yields (Φ_{PL} = 79-83 % in chloroform)[38] and bright green fluorescence, which coincides with the maximum in the IPCE (incident-photon-to-current-efficiency) spectrum of an N719-sensitised DSSC. The resultant LSCs (10 cm × 9 cm × 0.3 cm) are comparable in size to the largest area LSCs previously reported[1, 2] and are able to concentrate solar radiation with reasonable optical efficiencies under full AM1.5G spectral illumination in the absence of diffusers/reflectors. The effect of the luminophore concentration on the optical efficiency is investigated, along with the relative contributions of reabsorption and scattering processes along the length of the device. The inhomogeneity in the optical power output along the edge of the LSC is explored and we show that extrapolation of the edge emission can lead to erroneous values of the optical efficiency for large area devices, indicating the need for caution in these measurements. Finally, we present proof-of-principle integration of a QD-LSC with a planar, thin strip DSSC to generate an enhanced photocurrent.

Experimental Section

Materials

Cadmium acetate (anhydrous), zinc oxide, sulfur, selenium (99.99%), oleylamine (97 %), 1-octadecene, trioctylphosphine (97%), zinc acetate dihydrate, lauryl methacrylate, 2,2-dimethoxy-1,2-diphenylethan-1-one, 1-butyl-3-methyl imidazolium iodide (0.6 mol L^{-1}) iodine (0.03 mol L^{-1}), guandinium thiocyanate (0.10 mol L^{-1}) and 4-*tert*-butylpyridine were purchased from Sigma Aldrich. Ethylene glycol dimethacrylate was purchased from Santa Cruz Biotechnology. For fabrication of the DSSCs, TiO_2 paste, Pt paste (platisol) the adhesive surlyn gasket and the N719 sensitising dye (*cis*-di(thiocyanato)-*N*-*N*'-bis(2,2'-bipyridyl-4-carboxylicacid-4'-tetrabutylammonium carboxylate) ruthenium (II)) were purchased from Dyesol Ltd. All chemicals were used as received.

Synthesis of CdSe@ZnS/ZnS Quantum Dots

The synthesis of the CdSe@ZnS/ZnS QDs was performed using a scaled-up version of the procedure outlined by Lee *et al*.[38] In a single step, 0.42 mmol (0.1119 g) of $Cd(CH_3CO_2)_2$ and 10.23 mmol (0.834 g) of ZnO were mixed with oleylamine (OA, 21 mL) in a 200 mL three-neck round-bottom flask. This mixture was degassed at 150 °C for 30 min and then placed under an argon

atmosphere. Following this, degassed 1-octadecene (ODE, 45 mL) was injected, and the solution was heated to 310 °C. Upon reaching this temperature, (Se/S)-trioctylphosphine (TOP, 6.0 mL) was swiftly injected and 10 min were allowed to elapse to initiate the growth of CdSe@ZnS QDs. The (Se/S)-TOP stock solution was prepared by dissolving Se (15 mmol, 1.185 g) and S (15 mmol, 0.4809 g) in TOP (15 mL).

Following this, growth of the ZnS shell was undertaken by injecting S (4.8 mmol, 0.1539 g) dissolved in ODE (7.2 mL) into the growth solution of CdSe@ZnS QDs at 310 °C, followed by a growth time of 12 min. Next, Zn acetate dehydrate (8.58 mmol, 1.575 g) was dissolved in a mixture of OA (3 mL) and ODE (12 mL) and injected into the reaction mixture at 310 °C, after which the temperature of reaction was lowered to 270 °C. Finally, S (28.95 mmol, 0.9483 g) dissolved in TOP (15 mL) was added drop-wise at a rate of ~0.5 mL min^{-1} and the growth of the additional ZnS shell continued at 270 °C for a further 20 min.

Purification of CdSe@ZnS/ZnS Quantum Dots

The resulting CdSe@ZnS/ZnS QDs were precipitated by the addition of 1:5 MeOH:EtOH (100 mL) and separated through centrifugation (10 min, 4,000 rpm). Following this, the precipitate was dissolved in a minimum volume of hexane, and re-precipitated using a 10:1 EtOH:MeOH mixture. This step was repeated twice. The precipitated QDs were then re-dispersed in a minimum volume of hexane, after which acetone was added to the sample giving a 1:1 ratio of acetone to hexane. The QDs were then separated from solution using high-speed centrifugation (15,000 rpm) for 10 min. This step was repeated twice more. Following this, the QDs were dispersed in hexane (30 ml) and separated from solution *via* centrifugation at 15,000 rpm for 30 min. The QDs were then dissolved in hexane ready for use.

Fabrication of Large Area QD-LSCs

Un-doped LMA-*co*-EGDM co-polymer was prepared using the following protocol: lauryl methacrylate (LMA) (80 wt%) and ethylene glycol dimethacrylate (EGDM) (20 wt%) were added to a 3-neck round-bottom flask and stirred continuously at room temperature. The photoinitiator, 2,2-dimethoxy-1,2-diphenylethan-1-one (IGACURE 651), was added to this solution at 1 wt%. This prepolymerised solution was ultrasonicated for approximately 30 min to ensure adequate dispersion of the components throughout the mixture. The mixture was then degassed under vacuum-assisted ultrasonication for 1 h to ensure removal of residual oxygen from the mixture.

A homebuilt mould was developed to enable the fabrication of reproducible LSC plates (see **Figure S1** in the Electronic Supplementary Information (ESI)†). The mould consisted of a cavity created between two optically transparent glass plates. The cavity between the glass plates was sealed using a strip of poly(vinylchloride) (PVC) wire (~4mm thick), which acted as an impenetrable gasket. The glass moulding plates were held in place using spring-loaded clamps. The pre-polymerised solution was injected into the cavity the glass plates. Following injection, excess PVC gasket was used to seal the cavity; this ensured that the external atmosphere did not enter the cavity during the photopolymerisation reaction. Photopolymerisation was initiated by illuminating the top surface of the polymerisation chamber with UV radiation (366 nm) for up to 90 min; the polymerisation chamber was frequently inverted to ensure uniform illumination of the polymerisation matrix through both faces. Upon completion of the reaction, the clamps were carefully removed from the glass plates, the PVC gasket was slowly opened and the top glass plate removed from the moulding chamber. This allowed a freestanding LMA-*co*-EGDM slab to be removed, which was subsequently cured with UV radiation (366 nm) for 30 min.

For QD-doped LMA-*co*-EGDM LSCs the same curing procedure was employed. The QD-doped prepolymerised solutions were first prepared by adding the desired volume of QD stock solution in hexane to a vessel and removing the solvent by vacuum. Following this, a volume of LMA (typically 40-50 mL) was added, and sonicated to aid dissolution. To this mixture, EGDM and IGACURE-651 were added to make a 50 mL solution, which was then degassed with vacuum-assisted ultrasonication, and backfilled with Argon before curing as described above.

Characterisation of QD-LSCs and QD-LSC-DSSCs

The optical power output (OP_{out}) of the LSCs was evaluated using a Class AAA solar simulator (Oriel Sol3A) calibrated against a KG5-filtered reference diode (Oriel 91150-KG5) until an illumination of 1 sun (1000 $\pm$ 20 W m^{-2}) with an output beam size of *ca.* 10.16 $\times$ 10.16 cm (103.2 cm^2) was obtained. The optical power output at each edge of the LSC was measured by collecting the emitted light at the port of an integrating sphere (INS 125) coupled to an ILT 950 spectroradiometer. A variety of irradiation and collection geometries were evaluated (see **Figure 4** and Results and Discussion for more details). The optical power is extracted from the data measured by the spectroradiometer using Spectrolight III software, which utilises a suitable calibration file (ILT1007131U1INS125) for optical power measurements.

Reabsorption losses were evaluated using a Class ABB solar simulator (Abet Technologies) equipped with an AM 1.5G filter and suitable for small area illumination (9.6 cm^2) in conjunction with the integrating sphere and spectroradiometer set-up described above. The distance between the top face of the LSC and the illumination source was calibrated using a reference Si solar cell (ReRa Technologies) until an illumination of 1 sun (990 $\pm$ 30 W m^{-2}) was obtained. A black mask was used to confine irradiation of the top surface to a single circular spot (diameter = 4 cm) which was systematically moved from the centre to the LSC to the edge to vary the optical path length. Relative reabsorption losses were determined from the integrated OP_{out} spectrum measured at the centre of a single edge using a 4 cm port on the integrating sphere. The optical scattering properties of the pLMA-*co*-EGDM slab were analysed using a collimated beam (diameter = 4 cm) of light centred at 750 nm, which was generated by attaching a 750 nm band pass filter (THOR Labs) to the output terminal of the same solar simulator. The optical pathlength was varied as described for the reabsorption loss measurement.

Journal Name

ARTICLE

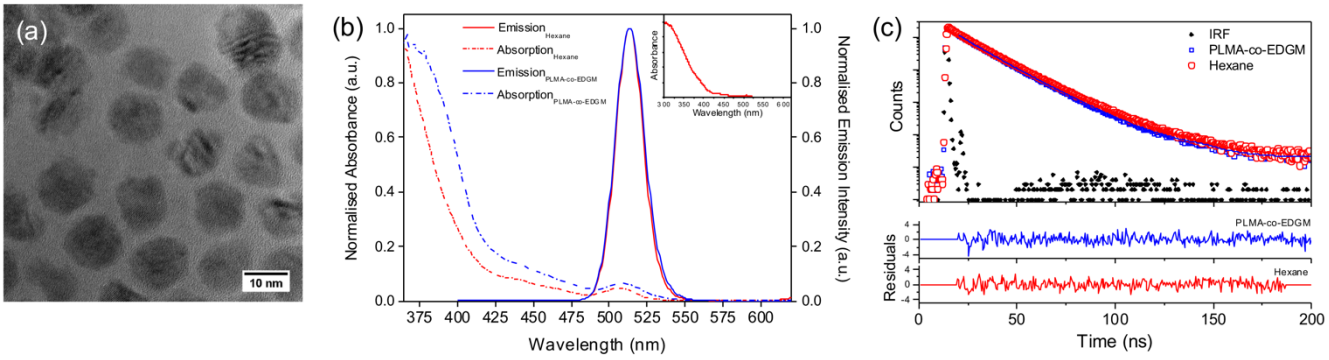

Figure 2 Physical and optical characterisation of CdSe@ZnS/ZnS QDs. (a) High resolution transmission electron microscope image (HRTEM) of CdSe@ZnS/ZnS QDs drop-cast from hexane onto a lacy carbon grid. The average particle size was determined to be 12.9 nm ± 1.7 nm (n = 400). (b) UV/Vis absorption and photoluminescence (PL) spectra (λ_{ex} = 350 nm) of CdSe@ZnS/ZnS QDs dissolved in hexane (red dashed/solid line) and embedded in a pLMA-*co*-EGDM film (blue dashed/solid line). The inset highlights the broad absorption profile of the QDs with the observation window extended to 300 nm. (c) PL decay curves of CdSe@ZnS/ZnS QDs in hexane (open red circles), the pLMA-*co*-EGDM matrix (open blue squares) and the instrument response function (IRF, black diamonds). Emission and excitation wavelengths were λ_{em} = 510 nm and λ_{ex} = 458 nm, respectively. Solid lines show the corresponding fits and residuals to a bi-exponential decay function

Accelerated photodegradation studies were performed by illuminating a thin strip QD-LSC (35 mm × 20 mm) with UV radiation (366 nm, 5.01 Wm^{-2}) at a fixed distance. The optical power of the UV source was determined using a photodiode (Newport, 818-UV-L detector) coupled to a Keithley 2401 source meter. Full details of the fabrication and characterisation methods used to prepare the thin strip DSSC and integrated QD-LSC-DSSC device can be found in the ESI†.

Results and Discussion

Characterisation of CdSe@ZnS/ZnS polymer composites

CdSe@ZnS/ZnS QDs with a composition gradient shell were synthesised using a modified hot-injection approach.[38] High resolution transmission electron microscopy (HRTEM) measurements reveal a monodisperse distribution of spherical nanoparticles, which exhibit distinct lattice fringes, thus indicating a high degree of crystallinity (**Figure 2a**). The mean particle diameter was 12.9 nm ± 1.7 nm (n = 400) (**Figure S3**, ESI†), which is in good agreement with the literature.[38] Energy dispersive X-ray (EDX) spectroscopy confirmed the chemical composition of the nanoparticles (**Figure S4**, ESI†).

The UV/Vis absorption and photoluminescence (PL) spectra of CdSe@ZnS/ZnS QDs in hexane and embedded in a pLMA-*co*-EGDM composite (~2.5 mm thick) are shown in **Figure 2b**. The UV/Vis absorption spectrum exhibits two distinct features: a small first excitonic band centred at 506 nm, assigned to absorption of the CdSe core, and a significantly more intense broad shoulder below 400 nm attributed to the onset of absorption for the ZnS shell.[38] This shoulder extends through the UVA to the UVB region to ~300 nm (**Figure 2b**, inset), highlighting the broad absorption window of these QDs. The position of the CdSe first excitonic band is moderately red-shifted (507 nm) when the QDs are embedded within the pLMA-*co*-EGDM matrix. This red-shift is commonly observed when studying the optical absorption properties of nanostructured objects in the solid-state and is most commonly associated with optical scattering of the incident light.[39, 40] The moderate overlap between the absorption of the first excitonic band (CdSe) and the emission spectrum suggests that reabsorption processes may be expected in the resultant LSC devices.

The PL spectra for CdSe@ZnS/ZnS QDs are essentially identical in solution and the polymer matrix, exhibiting a narrow emission band centred at 513 nm and a full-width-half-maximum (FWHM) of 21.35 nm and 22.55 nm, respectively. This indicates that the radical polymerisation process used to form the pLMA-*co*-EGDM matrix does not significantly affect the optical characteristics of the QDs. The photoluminescence quantum yield was determined to be Φ_{PL} = 65 (± 3.4 %) for CdSe@ZnS/ZnS QDs dispersed in hexane (see **Table S1**, ESI†, for further information). The radiative decay pathway was further investigated by examining the PL decay dynamics. Almost identical emission decay curves were obtained for CdSe@ZnS/ZnS QDs in hexane and the pLMA-*co*-EGDM matrix (**Figure 2c**). The decay profiles were fitted with a biexponential decay function, yielding observed lifetimes of τ_1 = 9.8 (±0.2) ns and τ_2 = 14.9 (±0.1) ns in the polymer composite, and τ_1 = 10.6

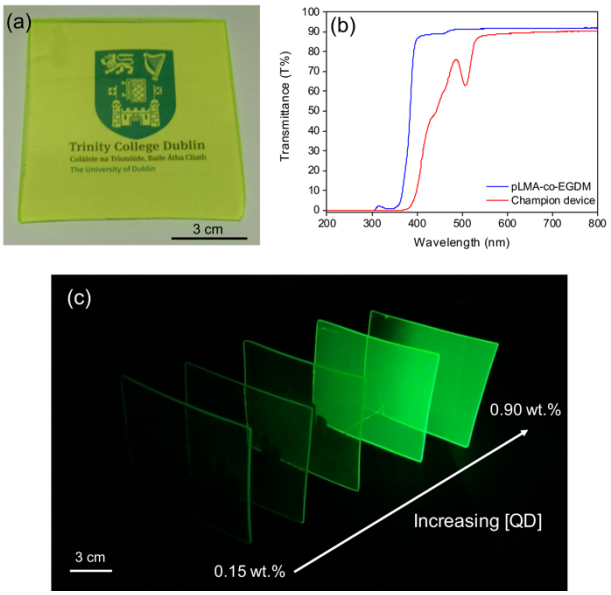

Figure 3. Optical properties of CdSe@ZnS/ZnS-LSCs. (a) Optical image of a QD-loaded LSC under standard indoor lighting conditions. (b) Optical transmission of an undoped pLMA-co-EGDM slab (~2.5 mm thick) and CdSe@ZnS/ZnS-LSC (0.9 wt%, ~2.5 mm thick).

(±0.2) ns and τ_2 =16.2 (±0.1) ns in solution. Previously, the deposition of CdSe@ZnS/ZnS QDs as a 40 nm-thick film was shown to result in a significant reduction in the observed lifetime (27.2 ns and 9.2 ns in solution and the film respectively), which was attributed to the introduction of additional non-radiative processes such as energy transfer and/or the exposure to an inhomogeneous environment.[38] The comparable decay dynamics observed here on going from solution to the solid-state confirm the absence of additional non-radiative decay channels, indicating that the excitonic emission is neither affected by the dispersion of the CdSe@ZnS/ZnS QDs within the polymer composite nor by the action of the radical initiator used to form it. The PL decay curve for QDs in the pLMA-*co*-EGDM matrix was recorded for a sample that was stored in a non-polymerised solution mixture for six weeks prior to polymerisation and characterisation, highlighting that the QDs are stable in the presence of the copolymer and the initiator for extended time periods.

Fabrication and characterisation of large area QD-LSCs

In order to evaluate the potential of CdSe@ZnS/ZnS core-shell QDs as luminophores for LSCs, six large area devices (~10 × 9 × 0.3 cm) were fabricated, in which the QD loading was varied between 0-0.9 wt%. pLMA-*co*-EGDM (80:20 wt%) was chosen as the polymer waveguide as it allows for facile design of QD-loaded polymer slabs, which retain high optical quality and minimise QD aggregation in the matrix,[6, 30] a problem often observed with hosts such as PMMA.[41-43] The as-produced CdSe@ZnS/ZnS LSCs exhibit high optical transparency under standard indoor illumination conditions (**Figure 3a**) and across the visible spectrum (88 %T at 550 nm, **Figure 3b**). This property is crucial for the application of such devices in BIPV and for the development of smart solar windows, which allow transmitted light to be used for indoor lighting or secondary solar harvesting applications.[3, 4] **Figure 3c** shows the concentrated green emission from the CdSe@ZnS/ZnS QDs which can clearly be observed from the slab edges upon illumination at 365 nm. As the concentration of QDs incorporated within the slab is increased (0.15-0.90 wt%), the observed intensity of the green fluorescence also increases.

The most commonly used figure-of-merit to describe the performance of an LSC is the optical conversion efficiency, η_{opt}, which is given by:

$$\eta_{opt} = \frac{OP_{out}}{OP_{in}} \quad (1)$$

where OP_{out} is the total optical power output obtained over the sum of the four edges of the LSC and OP_{in} is the incident optical power falling on the top surface of the slab. However, currently there is no standardised protocol for experimentally-determining η_{opt} in the research community, which can make it challenging to benchmark the performance of devices between laboratories. Moreover, an experimental approach that works well for small scale prototypes may not be directly applicable to larger devices. In this study, we used an integrating sphere (IS) coupled to a spectroradiometer to measure the optical power output at each edge of the LSC (see **Figure S6,** ESI†), an approach which is used by a number of research groups.[13, 14, 17] A limitation of this method is that the collection area is restricted by the size of the entry port to the IS. Here, we have evaluated a variety of collection geometries in order to explore the homogeneity of the concentrated emission across the edge length and the consequences of this on the subsequently calculated η_{opt} value. All measurements were performed using a dark background, without the use of reflective foil or scattering background to reflect photons emitted outside of the escape cone back into the waveguide for recycling. [2, 33]

In the first configuration, the entire top surface of the LSC was irradiated with calibrated solar simulated light (OP_{in} = 9000 mW over the 90 cm^2 top surface) and the emission was collected from the centre of the edge using a 4 cm entry port on the IS (**Figure 4a**). The captured spectrum was integrated between 250-1050 nm, and the value obtained was extrapolated to estimate OP_{out} for the entire edge length (9 or 10 cm). In the second geometry, the emission was collected across the entire edge length at consecutive increments using the 2 cm entry port on the IS (**Figure 4b**); OP_{out} was obtained from the sum of the integrated optical power obtained at each interval. In the final arrangement, the edge output was collected across the entire length, with 3 overlapping intervals using the 4 cm entry port (**Figure 4c**). These measurements were used to determine the mean integrated optical power for a 4 cm slice of the edge and this was extrapolated to obtain OP_{out} for the full edge length (9 or 10 cm).

Interestingly, differences in the measured edge output were identified depending on the size and position of the entry port to the IS across the edge length. As expected, the largest OP_{out} was obtained in the first measurement geometry, where the emission obtained from the edge centre is extrapolated to the full length (**Figure 4a**). However, on closer examination using

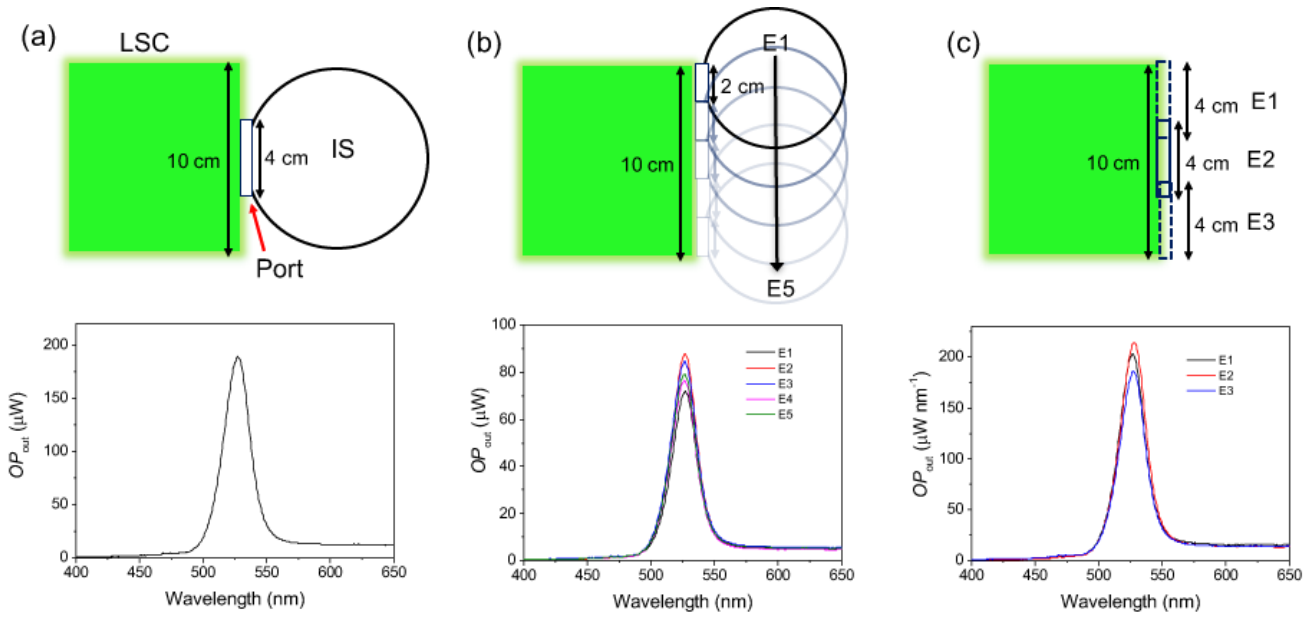

Figure 4. Top view of the different experimental geometries (not to scale) used to collect edge emission from QD-LSCs and the corresponding optical power spectra (OP_{out}) obtained with each configuration. The entire top surface of the LSC is irradiated with AM1.5G solar simulated light. In (a) the edge emission is collected at the centre of the LSC using a 4 cm port to the integrating sphere (IS). The integrated OP_{out} (250-1050 nm) value is extrapolated to estimate a value for the full edge length (9 or 10 cm). (b) OP_{out} spectra are collected across the full edge length by moving the IS at 2 cm intervals. The integrated OP_{out} (250-1050 nm) at each interval is summed to give the total edge OP_{out}. (c) OP_{out} spectra are collected across the full edge length using three overlapping intervals (4 cm). The mean integrated OP_{out} (250-1050 nm) is determined and extrapolated to estimate a value for the full edge length (9 or 10 cm). The data presented are for the 0.7 wt% QD-LSC.

the arrangement shown in **Figure 4b**, it becomes apparent that the emission is in fact not homogeneous across the edge length, with the maximum intensity measured at the edge centre (Edge 3), which drops off as the entry port is moved towards the edge extremity. This clearly indicates that the extrapolation method used in the first arrangement overestimates the edge output, and this becomes more significant as the size of the LSC is increased. However, fluctuations in the measured power output were also observed using geometry 2. Notably, for the same edge region, the sum of the emission measured consecutively using the 2 cm port twice led to a significantly lower output than a single measurement using the 4 cm port at the same edge location. This is understandable, since accurate alignment of the port to perform sequential measurements proved difficult. This factor, coupled with increased number of measurements required using the smaller port, inherently leads to a greater systematic error in the data obtained using this approach.

The geometry illustrated in **Figure 4c** overcomes these limitations, taking into account the non-homogeneity of the emission across the edge, while eliminating the systematic errors introduced by using the smaller port. The calculated η_{opt} values obtained for all CdSe@ZnS/ZnS LSCs as a function of luminophore concentration using this approach are presented in **Table 1** (see **Table S2**, ESI† for individual measurement data). At low QD concentrations (<0.55 wt%), η_{opt} is comparable within experimental error. However, as the QD loading is increased further, η_{opt} also increases reaching a maximum value of 1.22% for a loading of 0.9 wt%. This value is well within the theoretical upper limit for the optical efficiency of this system, which is around 6% (see ESI†).[44] The increase in η_{opt} with QD concentration suggests that the threshold for η_{opt} is not yet achieved at the dopant concentrations studied and that any decrease in the optical efficiency due to reabsorption is determined primarily the intrinsic spectral overlap integral of the luminophore rather than the nearest neighbour distance. We note that higher dopant concentrations lead to incomplete polymerisation of the pLMA-*co*-EGDM matrix, even with extended curing time.

Table 1. Optical efficiencies (η_{opt}) obtained for CdSe@ZnS/ZnS LSCs under 1 sun illumination. OP_{out} is the sum of the optical power measured for each edge as described in the text.

QD concentration (wt%)	OP_{out} (mW)[a]	η_{opt} (%)[b]
0	46.0	0.51
0.04	47.9	0.53
0.15	48.4	0.54
0.30	50.8	0.56
0.55	56.9	0.63
0.70	106.3	1.18
0.90	109.8	1.22

[a] Sum of OP_{out} measured for each edge using the arrangement shown in Figure 4c. [b] Determined from Eq. 1 using OP_{in} = 9000 mW (90 cm² × 100 mW/cm²).

The variety of different device architectures used in previous studies of QD-LSCs makes direct comparison of the performance difficult. However, for planar and thin film LSCs, the influence of the dimensions of the LSC on the optical

Journal Name

ARTICLE

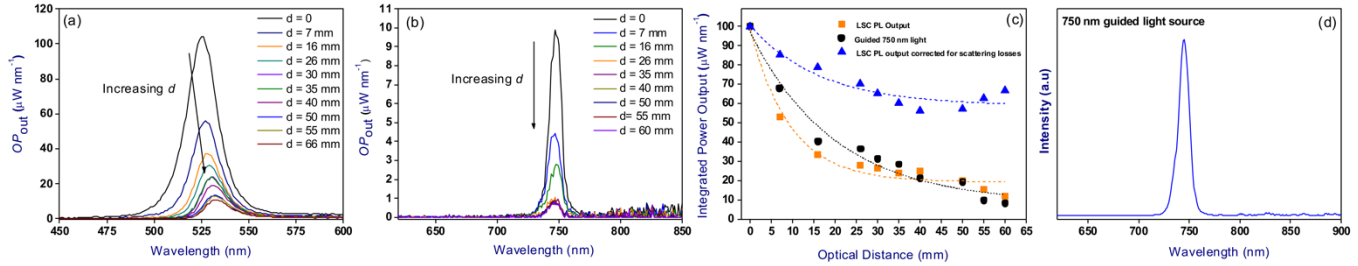

Figure 5. Determination of reabsorption and scattering losses in the champion CdSe@ZnS/ZnS-LSC (0.9 wt%). (a) Optical power output (OP_{out}) at the centre of a single edge (4.0 × 0.3 cm) as a function of distance, *d*, from the illumination site under irradiation with solar simulated light (1 sun). The black arrow highlights the red shift (525 –530 nm) and decrease in optical power observed with increasing *d* due to the reabsorption of emitted photons. (b) Optical power output under the same measurement conditions using guided 750 nm light. The black arrow highlights the decrease in optical power but absence of red-shift with increasing *d* using this irradiation source. (c) Intensity normalised decay of the integrated optical power output as a function of *d* under 1 sun illumination (orange squares) and using 750 nm guided light (black circles). The calculated integrated optical power output corrected for scattering losses (blue triangles) is also shown. The dashed lines represent an exponential fit to the data. (d) Spectral profile of the 750 nm source used for the guided light experiments

efficiency can be accounted for by the geometric gain factor, *G*, is given by:[6, 45]

$$G = \frac{A_{\text{surface}}}{A_{\text{edge}}} \quad (2)$$

where $A_{surface}$ and A_{edge} are the area of the top surface and total area of the summed edges of the LSC, respectively. It is well-documented in the literature that η_{opt} decreases with increasing *G* values;[32] hence it is important for *G* values to be expressed with conformity in the literature.

The overall performance of an LSC, taking into account the optical efficiency and the LSC geometry, can thus be quantified by the concentration factor, *F*:[45]

$$F = \eta_{opt} G \quad (3)$$

For the CdSe@ZnS/ZnS LSCs fabricated in this work, a value of *G* = 7.9 is obtained, with a max. η_{opt} = 1.2%. This corresponds to a concentration factor of *F*= 0.10. For comparison, the recent work by Zhou *et al*. reported an η_{opt} of 6.1% for a PbS/CdS-doped QD LSC, where *G* = 2.14 if the contribution from all 4 edges of the slab is considered, and *F* = 0.15.[33] Similarly, using the same approach for the CdSe/CdS LSC reported by Meinardi *et al.*, a *G* value of 1.22 is obtained and η_{opt} = 10.2 %, with *F* = 0.12.[2] Large area, planar LSCs have also been fabricated by Meinardi *et al.* utilising $CuInSe_xS_{2-x}$ QDs, with a reported efficiency of 3.2% when *G* = 10, leading to *F* = 32.[1]

Optical loss mechanisms

The moderate overlap between the absorption and emission spectra of the CdSe@ZnS/ZnS QDs (**Figure 2b**) suggests that reabsorption processes may contribute to a decrease in the optical efficiency of the LSCs. However, additional loss mechanisms including light scattering by the embedded QDs and imperfections present in the host matrix may also affect the device performance.[5] The influence of reabsorption and scattering losses to the champion CdSe@ZnS/ZnS-LSC output is shown in **Figure 5**. Reabsorption losses were determined from the OP_{out} at the centre of a single edge for the LSC as a function of the optical pathlength from the irradiation spot, *d*, under 1 sun illumination. As *d* increases, the PL output gradually decreases and a slight red-shift in the emission maximum (from 525 nm to 530 nm) is observed up to *d* = 30 mm (**Figure 5a**). At greater distances the position of the emission maximum remains relatively unchanged, suggesting that optical losses due to self-absorption are saturated for optical distances > 30 mm.

To isolate scattering losses from reabsorption, the optical edge output of the LSCs was also monitored as a function of *d,* using monochromatic light centred at 750 nm. Since CdSe@ZnS/ZnS QDs do not absorb at this wavelength (**Figure 2b**), any losses in the optical output can be attributed to scattering from either polymer matrix defects and/or the QDs. A similar decrease in the OP_{out} was detected with increasing optical pathlength (**Figure 5b**). However, the red-shift in the emission maximum was no longer observed, confirming that reabsorption effects are negligible in this wavelength region. Under both illumination conditions (1 sun or 750 nm), the optical power decays exponentially with increasing distance from the illumination point, decreasing to ~10-15 % of the initial power output for *d* > 50 mm. The contribution of reabsorption to the optical efficiency can therefore be isolated by subtracting for scattering losses at a given *d*, as shown in **Figure 5c**. Using

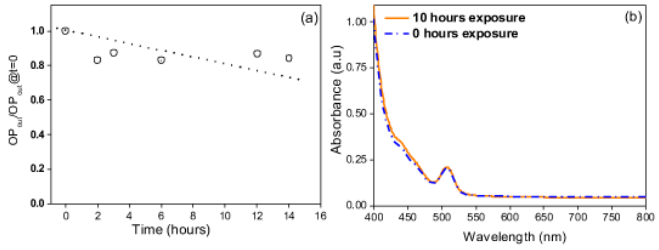

Figure 6 Accelerated photodegradation of a CdSe@ZnS/ZnS-LSC (35 mm × 20 mm) under high intensity UV radiation (366 nm, 5.01 Wm^{-2}). (a) Optical power output as a function of irradiation time (normalised to OP_{out} at 0 h irradiation). (b) UV/Vis absorption spectra obtained after 0 h (blue line) and 10 h (orange line) UV illumination.

this approach reabsorption losses are estimated to be ~40% at optical distances up to 65 mm from the irradiation centre.

Photostability

The photostability of the CdSe@ZnS/ZnS-LSC was evaluated by examining changes in the optical properties after prolonged periods of exposure to high intensity UV radiation (366 nm, 5.01 Wm^{-2}). Accelerated photodegradation of the LSC was monitored by measuring the optical power output (under 1 sun illumination) and UV/Vis absorption spectrum as a function irradiation time. As shown in **Figure 6a**, the OP_{out} decreases by only 20% after extended irradiation periods (14 h). This result highlights the advantage of utilising QDs in LSC applications, when compared to traditional organic luminophores, which are known to degrade rapidly when exposed to high intensity UV radiation.[14] The UV/Vis absorption spectrum of the LSC (**Figure 6b**) confirms that no other photoactive species is generated during the irradiation process. No significant change in the excitonic peak position or intensity was observed after 10 hours of exposure, confirming the stability of the QDs to high intensity UV exposure. Similar trends have been made by Zhou *et al*,[33] who reported high levels of photostability for QD-based LSCs.

Integration with third generation photovoltaic technologies

In order for an LSC to operate effectively as an energy-harvesting device, the LSC needs to be coupled with an appropriate solar cell. Ideally, the chosen solar cell will operate with a high external quantum efficiency in the wavelength range of the emission frequency of the LSC and hence, light emitted from the edges of the LSC can be captured efficiently, producing the maximum photocurrent. The literature to date is dominated with examples of LSCs coupled to Si solar cells; [13, 14, 43] however, few attempts have been made at coupling LSCs to other classes of PV cells. This is most likely due to the limited exploration of LSCs containing luminophores whose emission properties are compatible with the spectral response of emerging PV technologies such as DSSCs and perovskite solar cells and also the challenge of fabricating prototypes of such devices in the required format. For example, Peng *et al.* have reported on the integration of fibre DSSCs (FDSC) with commercially-available LSCs, demonstrating an increase in efficiency for the FDSCs coupled to both red- and green-emitting LSCs.[34, 35] Further attempts have been made at increasing the short-circuit current density of DSSCs with the use of luminescent down-shifting (LDS).[46-49] The application of LDS layers has also been

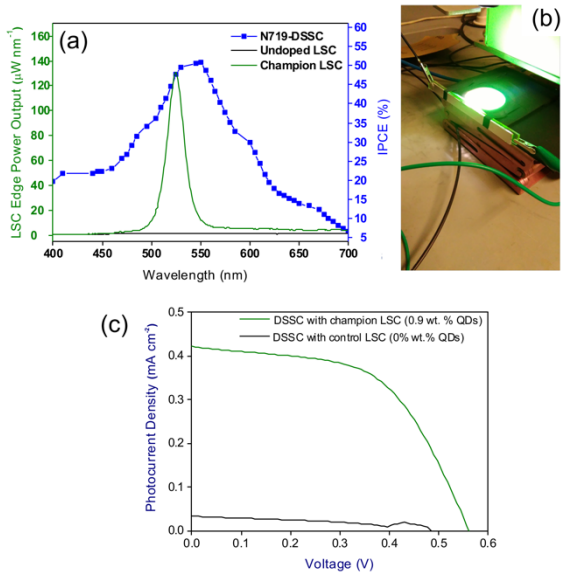

Figure 7 Characterisation of an integrated CdSe@ZnS/ZnS-LSC-DSSC device. (a) Edge emission for the champion LSC device (green) and an undoped pLMA-*co*-EGDM slab (black) and the IPCE spectrum of an N719 DSSC. All measurements performed under 1 sun illumination with an edge area of 0.4 × 0.3 cm^2 for the LSCs. (b) Photograph of the integrated CdSe@ZnS/ZnS-LSC-DSSC device. (c) Current-voltage characteristics of the DSSC obtained following illumination of either the champion LSC (green) or a control device (undoped pLMA-*co*-EGDM slab, black).

investigated for emerging PV technologies, such as perovskite solar cells, whereby unabsorbed UV light is down-shifted to optical frequencies that can be harnessed by the absorber.[37]

In an effort to address this gap, we have integrated a CdSe@ZnS/ZnS LSC with a thin strip DSSC to demonstrate proof-of-conept viability of this approach. The champion LSC (η_{opt} = 1.2%) exhibits an emission maximum centred at 520 nm in the single edge optical power output spectrum (**Figure 7a**). This coincides well with the IPCE spectrum recorded for an N719-sensitised DSSC (1 cm × 1 cm), where N179 is the commonly used sensitiser dye di-tetrabutylammonium *cis*-bis(isothiocyanato)bis(2,2'-bipyridyl-4,4'dicarboxylato)ruthenium(II)).[50, 51] The optical power obtained from an undoped LSC (*i.e.* a blank pLMA-*co*-EGDM slab of the same dimensions) is also shown for comparison and confirms that the waveguide host makes zero contribution to the optical output of the slab in the visible region.

To quantify the ability of the CdSe@ZnS/ZnS LSCs to effectively sensitise an N719-DSSC, a thin strip DSSC (active area = 9 × 0.2 cm) was fabricated and coupled to the edge of the champion LSC (**Figure 7b**). The LSC was illuminated by a calibrated solar simulator (AM 1.5G) and the current-voltage (*J-V*) performance of the attached DSSC was measured. Notably, the short-circuit current density obtained for the CdSe@ZnS/ZnS LSC-DSSC device, J_{SC} = 0.42 mA cm^{-2}, was greater than the corresponding photocurrent recorded for the undoped pLMA-*co*-EGDM slab (J_{SC} = 0.032 mA cm^{-2}) (**Figure 6c**). Given the large dimension of our thin-strip DSSC, it was difficult to obtain an accurate value for the overall efficiency of the bare device, since only partial illumination of the front face of the DSSC was

possible with our experimental configuration. However, the power conversion efficiency (PCE) of the DSSC upon sensitisation by the edge emission of the coupled LSC can be estimated from:

$$PCE = \frac{I_{SC} V_{OC} FF}{OP_{in}} \quad (4)$$

where I_{SC} is the short-circuit current (0.76 mA), V_{OC} is the open-circuit voltage (0.56 V) and *FF* is the fill factor (0.55). Here, OP_{in} is taken to be the optical power of the corresponding LSC edge emission (8.64 mW), which gives a PCE of 2.71% for the DSSC.

Conclusions

In summary, we have successfully fabricated large-area LSCs utilising green-emitting CdSe@ZnS/ZnS QDs with a composition gradient shell as the luminophore. Judicious selection of pLMA-*co*-EGDM as the waveguide slab facilitated the incorporation of the CdSe@ZnS/ZnS QDs to high dopant concentrations (up to 0.9 wt%), without affecting the intrinsic photophysical properties of the QDs. The semitransparent CdSe@ZnS/ZnS-LSCs display high optical quality and demonstrated a maximum operating efficiency of 1.2 % for a geometric factor of G = 7.9 under AM 1.5G illumination (250 nm-1050 nm). We note that additional light scattering or reflective layers are not employed to achieve this result. It was observed that the edge emission exhibits considerable inhomogeneity across the edge length, which can lead to significant overestimation of the optical power output if it is not accounted for. Several measurement geometries have been evaluated to compensate for this and we propose that a suitable approach for large area devices is to determine the mean edge emission from multiple overlapping intervals over the entire edge length. This approach minimises systematic errors, whilst accounting for the inhomogeneity in the edge emission.

Evaluation of the contribution of optical losses to the efficiency has shown that reabsorption losses reach ~40% at optical distances > 60 mm. The champion LSC was integrated with a DSSC and was shown to boost the short-circuit photocurrent, when compared to an undoped polymer slab. To the best of our knowledge, this is the first reported example of a QD-LSC coupled to a planar DSSC. Given that emerging PV technologies such as DSSCs, organic and perovskite solar cells have been heralded as low-cost, lightweight alternatives to established inorganic semiconductor PV cells for the urban environment, this work highlights the significant opportunity for the rational design of hybrid LSC/PV systems where third generation solar cells are a viable prospect.

Conflicts of Interest

There are no conflicts of interest to declare.

Acknowledgements

This work was supported by the Science Foundation Ireland under Grants No. 12/IP/1608, 12/IA/1300 and 14/TIDA/2343. The authors would like to thank the reviewers for their insightful feedback during the evaluation stage.

References

1. F. Meinardi, H. McDaniel, F. Carulli, A. Colombo, K. A. Velizhanin, N. S. Makarov, R. Simonutti, V. I. Klimov and S. Brovelli, *Nat. Nanotechnol.*, 2015, **10**, 878-885.
2. F. Meinardi, A. Colombo, K. A. Velizhanin, R. Simonutti, M. Lorenzon, L. Beverina, R. Viswanatha, V. I. Klimov and S. Brovelli, *Nat. Photonics*, 2014, **8**, 392-399.
3. F. M. Vossen, M. P. Aarts and M. G. Debije, *Energ. Buildings*, 2016, **113**, 123-132.
4. M. Debije, *Nature*, 2015, **519**, 298-299.
5. M. G. Debije and P. P. Verbunt, *Adv. Energy Mater.*, 2012, **2**, 12-35.
6. F. Purcell-Milton and Y. K. Gun'ko, *J. Mater. Chem.*, 2012, **22**, 16687-16697.
7. B. McKenna and R. C. Evans, *Adv. Mater.*, 2017, 1606491.
8. M. Debije, *Nat. Photonics*, 2017, **11**, 143-144.
9. B. Swartz, T. Cole and A. Zewail, *Opt. Lett.*, 1977, **1**, 73-75.
10. A. Goetzberger and W. Greube, *Appl. Phys. A*, 1977, **14**, 123-139.
11. M. J. Currie, J. K. Mapel, T. D. Heidel, S. Goffri and M. A. Baldo, *Science*, 2008, **321**, 226-228.
12. F. Meinardi, S. Ehrenberg, L. Dhamo, F. Carulli, M. Mauri, F. Bruni, R. Simonutti, U. Kortshagen and S. Brovelli, *Nat. Photonics*, 2017, **11**, 177-185.
13. A. Kaniyoor, B. McKenna, S. Comby and R. C. Evans, *Adv. Opt. Mater.*, 2016, **4**, 444-456.
14. L. Desmet, A. Ras, D. De Boer and M. Debije, *Opt. Lett.*, 2012, **37**, 3087-3089.
15. M. Buffa, S. Carturan, M. Debije, A. Quaranta and G. Maggioni, *Sol. Energy Mater. Sol. Cells*, 2012, **103**, 114-118.
16. I. Meazzini, N. Willis-Fox, C. Blayo, J. Arlt, S. Clément and R. C. Evans, *J. Mater. Chem. C*, 2016, **4**, 4049-4059.
17. P. T. Albers, C. W. Bastiaansen and M. G. Debije, *Solar Energy*, 2013, **95**, 216-223.
18. W. G. van Sark, K. W. Barnham, L. H. Slooff, A. J. Chatten, A. Büchtemann, A. Meyer, S. J. McCormack, R. Koole, D. J. Farrell and R. Bose, *Opt. Express*, 2008, **16**, 21773-21792.
19. L. R. Bradshaw, K. E. Knowles, S. McDowall and D. R. Gamelin, *Nano Lett.*, 2015, **15**, 1315-1323.
20. S. F. Correia, V. de Zea Bermudez, S. J. Ribeiro, P. S. André, R. A. Ferreira and L. D. Carlos, *J. Mater. Chem. A*, 2014, **2**, 5580-5596.
21. X. Wang, T. Wang, X. Tian, L. Wang, W. Wu, Y. Luo and Q. Zhang, *Solar Energy*, 2011, **85**, 2179-2184.
22. V. T. Freitas, L. Fu, A. M. Cojocariu, X. Cattoën, J. R. Bartlett, R. Le Parc, J.-L. Bantignies, M. Wong Chi Man, P. S. André, R. A. S. Ferreira and L. D. Carlos, *ACS Appl. Mater. Interfaces*, 2015, **7**, 8770-8778.
23. J. L. Banal, K. P. Ghiggino and W. W. Wong, *Phys. Chem. Chem. Phys.*, 2014, **16**, 25358-25363.
24. J. L. Banal, J. M. White, K. P. Ghiggino and W. W. Wong, *Sci. Rep.*, 2014, **4**, 4635.
25. B. Mahler, P. Spinicelli, S. Buil, X. Quelin, J.-P. Hermier and B. Dubertret, *Nat. Mater.*, 2008, **7**, 659-664.
26. K. Yu, J. Ouyang, Y. Zhang, H.-T. Tung, S. Lin, R. A. Nagelkerke, D. Kingston, X. Wu, D. M. Leek and D. Wilkinson, *ACS Appl. Mater. Interfaces*, 2011, **3**, 1511-1520.
27. W. Zhang, Y. Li, H. Zhang, X. Zhou and X. Zhong, *Inorg. Chem*, 2011, **50**, 10432-10438.
28. Q. Wei, Y. Zhao, Q. Di, J. Liu, M. Xu, J. Liu and J. Zhang, *J. Phys. Chem. C*, 2017, **121**, 6152-6159.
29. G. Xu, Y. Li, Y. Qin, Z. Liu, J. Han, Y. Han and K. Yao, *Opt. Mater. Express*, 2015, **5**, 1460-1468.
30. J. Lee, V. C. Sundar, J. R. Heine, M. G. Bawendi and K. F. Jensen, *Adv. Mater.*, 2000, **12**, 1102-1105.
31. Y. Zhao and R. R. Lunt, *Adv. Energy Mater.*, 2013, **3**, 1143-1148.
32. C. S. Erickson, L. R. Bradshaw, S. McDowall, J. D. Gilbertson, D. R. Gamelin and D. L. Patrick, *ACS Nano*, 2014, **8**, 3461-3467.
33. Y. Zhou, D. Benetti, Z. Fan, H. Zhao, D. Ma, A. O. Govorov, A. Vomiero and F. Rosei, *Adv. Energy Mater.*, 2016, **6**, 1501913.
34. M. Peng, S. Hou, H. Wu, Q. Yang, X. Cai, X. Yu, K. Yan, H. Hu, F. Zhu and D. Zou, *J. Mater. Chem. A*, 2014, **2**, 926-932.
35. M. Peng, X. Yu, X. Cai, Q. Yang, H. Hu, K. Yan, H. Wang, B. Dong, F. Zhu and D. Zou, *Nano Energy*, 2014, **10**, 117-124.

36. Z. Hosseini, N.Taghavinia and E. W.-G. Diau, *Chem. Phys. Chem.*, 2017, **18**, 3292-3308.
37. N. Chander, A. Khan, P. Chandrasekhar, E. Thouti, S. K. Swami, V. Dutta and V. K. Komarala, *Appl. Phys. Lett.*, 2014, **105**, 033904.
38. K.-H. Lee, J.-H. Lee, H.-D. Kang, B. Park, Y. Kwon, H. Ko, C. Lee, J. Lee and H. Yang, *ACS Nano*, 2014, **8**, 4893-4901.
39. S. Cho, S. Jung, S. Jeong, J. Bang, J. Park, Y. Park and S. Kim, *Langmuir*, 2012, **29**, 441-447.
40. S. Cho, J. Kwag, S. Jeong, Y. Baek and S. Kim, *Chem. Mater.*, 2013, **25**, 1071-1077.
41. J. Bomm, A. Büchtemann, A. Fiore, L. Manna, J. H. Nelson, D. Hill and W. G. van Sark, *Beilstein J. Nanotechnol.*, 2010, **1**, 94.
42. J. Bomm, A. Büchtemann, A. J. Chatten, R. Bose, D. J. Farrell, N. L. Chan, Y. Xiao, L. H. Slooff, T. Meyer and A. Meyer, *Sol. Energy Mater. Sol. Cells*, 2011, **95**, 2087-2094.
43. N. D. Bronstein, L. Li, L. Xu, Y. Yao, V. E. Ferry, A. P. Alivisatos and R. G. Nuzzo, *ACS Nano*, 2013, **8**, 44-53.
44. H. Hernandez-Noyola, D. H. Potterveld, R. J. Holt and S. B. Darling, *Energy Environ. Sci.*, 2012, **5**, 5798.
45. S. F. H. Correia, P. P. Lima, E. Pecoraro, S. J. L. Ribeiro, P. S. André, R. A. S. Ferreira and L. D. Carlos, *Prog. Photovoltaics Res. Appl.*, 2016, **24**, 1178-1193.
46. F. Bella, G. Griffini, M. Gerosa, S. Turri and R. Bongiovanni, *J. Power Sources*, 2015, **283**, 195-203.
47. H. Ahmed, J. Doran and S. McCormack, *Solar Energy*, 2016, **126**, 146-155.
48. M. Kennedy, H. Ahmed, J. Doran, B. Norton, P. Bosch-Jimenez, M. D. Pirriera, E. Torralba-Calleja, D. G. Tauste, L. Aubouy and S. Daren, *Phys. Status Solidi A*, 2015, **212**, 203-210.
49. J. Liu, Q. Yao and Y. Li, *Appl. Phys. Lett.*, 2006, **88**, 173119.
50. M. Grätzel, *Inorg. Chem.*, 2005, **44**, 6841-6851.
51. M. Grätzel, *Nature*, 2001, **414**, 338-344.